JACS
JOURNAL OF THE AMERICAN CHEMICAL SOCIETY
Article
Cite This: J. Am. Chem. Soc. 2019, 141, 7320−7326
pubs.acs.org/JACS

Glutamine Side Chain $^{13}C{=}^{18}O$ as a Nonperturbative IR Probe of Amyloid Fibril Hydration and Assembly

Haifan Wu,[†] Daniel J. Saltzberg,[‡] Huong T. Kratochvil,[†] Hyunil Jo,[*,†] Andrej Sali,[*,‡] and William F. DeGrado[*,†]

[†]Department of Pharmaceutical Chemistry and the Cardiovascular Research Institute and [‡]Department of Bioengineering and Therapeutic Sciences, Department of Pharmaceutical Chemistry, and California Institute for Quantitative Biosciences (QB3), University of California, San Francisco, San Francisco, California 94143, United States

Supporting Information

ABSTRACT: Infrared (IR) spectroscopy has provided considerable insight into the structures, dynamics, and formation mechanisms of amyloid fibrils. IR probes, such as main chain $^{13}C{=}^{18}O$, have been widely employed to obtain site-specific structural information, yet only secondary structures and strand-to-strand arrangements can be probed. Very few nonperturbative IR probes are available to report on the side-chain conformation and environments, which are critical to determining sheet-to-sheet arrangements in steric zippers within amyloids. Polar residues, such as glutamine, contribute significantly to the stability of amyloids and thus are frequently found in core regions of amyloid peptides/proteins. Furthermore, polyglutamine (polyQ) repeats form toxic aggregates in several neurodegenerative diseases. Here we report the synthesis and application of a new nonperturbative IR probe—glutamine side chain $^{13}C{=}^{18}O$. We use side chain $^{13}C{=}^{18}O$ labeling and isotope dilution to detect the presence of intermolecularly hydrogen-bonded arrays of glutamine side chains (Gln ladders) in amyloid-forming peptides. Moreover, the line width of the $^{13}C{=}^{18}O$ peak is highly sensitive to its local hydration environment. The IR data from side chain labeling allows us to unambiguously determine the sheet-to-sheet arrangement in a short amyloid-forming peptide, GNNQQNY, providing insight that was otherwise inaccessible through main chain labeling. With several different fibril samples, we also show the versatility of this IR probe in studying the structures and aggregation kinetics of amyloids. Finally, we demonstrate the capability of modeling amyloid structures with IR data using the integrative modeling platform (IMP) and the potential of integrating IR with other biophysical methods for more accurate structural modeling. Together, we believe that side chain $^{13}C{=}^{18}O$ will complement main chain isotope labeling in future IR studies of amyloids and integrative modeling using IR data will significantly expand the power of IR spectroscopy to elucidate amyloid assemblies.

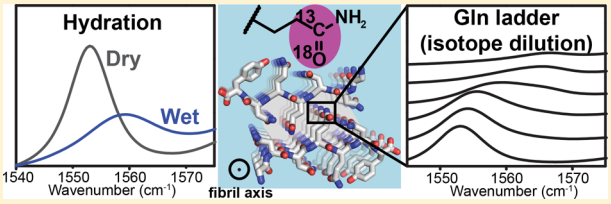

INTRODUCTION

Extensive efforts have been dedicated to understanding the structures, dynamics, and aggregation pathways of amyloid fibrils to inform principles underlining amyloid formation, strategies of inhibition, and designs of amyloid-based biomaterials.[1−4] High-resolution techniques, such as X-ray diffraction, microelectron diffraction (MicroED), solid-state NMR (ssNMR), and cryo-electron microscopy (cryoEM), have provided atomic details of amyloid assemblies,[5−13] yet they give few insights into the pathways of amyloid formation. By contrast, infrared (IR) spectroscopy is one of the few techniques that can probe not only amyloid structures and dynamics but also formation kinetics.[14−18]

A major drawback of IR spectroscopy is the lack of residue specificity, which can nevertheless be overcome through site-specific IR probes.[14,15] For instance, main chain $^{13}C{=}^{18}O$,[16,19,20] which red shifts the amide I band of a particular residue away from the congested main band, has been used to follow conformational changes at specific sites during amyloid aggregation[21,22] and to investigate strand-to-strand arrangements in amyloids;[23,24] however, little information is available to derive the tertiary and quaternary packing of amyloids. On the other hand, unnatural side chain probes, such as thiocyanates, azides, nitriles, and esters, have been employed to determine the intersheet packing, local electrostatic environment, and hydrogen bonding dynamics within amyloids.[15,25−29] These unnatural side chain probes are advantageous because of their distinctive IR absorption frequencies. However, the need to introduce unnatural groups[30] has greatly limited their application to amyloids because amyloid conformations are highly sensitive to even subtle changes.[31] Thus, we explored nonperturbative intrinsic side chain IR probes.

High-resolution structures of fibril-like microcrystals formed by short peptide segments have revealed the steric zipper as the basic unit of amyloid assembly and identified key motifs and interactions that stabilize amyloid structures.[3,32] One particular type of interaction involves side chains of polar residues, which form hydrogen-bonding networks to achieve extraordinarily

Received: January 17, 2019
Published: April 17, 2019

DOI: 10.1021/jacs.9b00577
J. Am. Chem. Soc. 2019, 141, 7320−7326

high stability.[5,6,33] As a critical residue in these polar interactions, glutamine is frequently observed in the core region of amyloid peptides/proteins.[34−37] Moreover, pathogenic mutations to Gln cause more rapid aggregation and are associated with earlier onsets of disease.[38,39] Furthermore, polyglutamine (polyQ) peptides form toxic aggregates in several neurodegenerative diseases.[40] Given the important role of glutamine residues in amyloids, the glutamine side chain amide is a promising intrinsic IR probe. However, it has never been explored because of a lack of isotope labeling strategies that can differentiate its absorption band from the main amide band. Thus, there is a great need for a synthesis method to introduce $^{13}C{=}^{18}O$ into the side chain of Gln regioselectively. Here we developed a synthesis methodology for selective and efficient $^{13}C{=}^{18}O$ labeling of the glutamine side chain. We found that this probe is highly sensitive to its arrangement and local hydration environment within amyloid fibrils. We also present the first attempt to use IR data in the integrative modeling of amyloid structures using the open source integrative modeling platform (IMP) program.[41]

RESULTS AND DISCUSSION

Robust Synthesis Method of Side-Chain $^{13}C{=}^{18}O$ Labeling. Previously, several strategies have been reported for the main chain $^{13}C{=}^{18}O$ labeling, including an acid-catalyzed ^{18}OH exchange[19,42] and the hydrolysis of an activated ester[43] (Figure 1a). Gai and co-workers also reported the ^{13}C labeling of an aspartate side chain via an asymmetric alkylation reaction.[44] However, these approaches have potential limitations in selective side chain $^{13}C{=}^{18}O$ labeling of glutamine. For instance, when applied to amides, the acid-catalyzed ^{18}OH exchange approach will cause many undesired side reactions. The hydrolysis of activated ester can provide only acid rather than the required amide side chain. Then it was envisaged that the hydration of nitrile by $H_2{}^{18}O$ could provide a solution. To test our strategy, we first performed a substitution reaction with $Na^{13}CN$ to give nitrile intermediate **2** in 73% yield (Figure 1b). It is also worth mentioning that this approach can provide one of the most affordable routes to the introduction of selective ^{13}C labeling on the side chain of Gln. For the key transformation, the hydrolysis of nitrile to amide, we employed the Ghaffar−Parkins catalyst[45] because its functional group selectivity has been demonstrated in total syntheses of a variety of natural products.[46−48] Gratifyingly, hydrolysis with ^{18}O water afforded $^{13}C{=}^{18}O$-labeled amide **3** in 88% yield, and isotopic enrichment was more than 95% by mass analysis (Figure S1). We then installed trityl (Trt) with Trt-OH catalyzed by concentrated H_2SO_4. The removal of Cbz, methyl ester, and fluorenylmethyloxycarbonyl (Fmoc) protection produced final product **5** in 88% yield over three steps. Our method provided 4 g of product ready for solid-phase peptide synthesis, and we foresee no difficulties in scaling the procedure further.

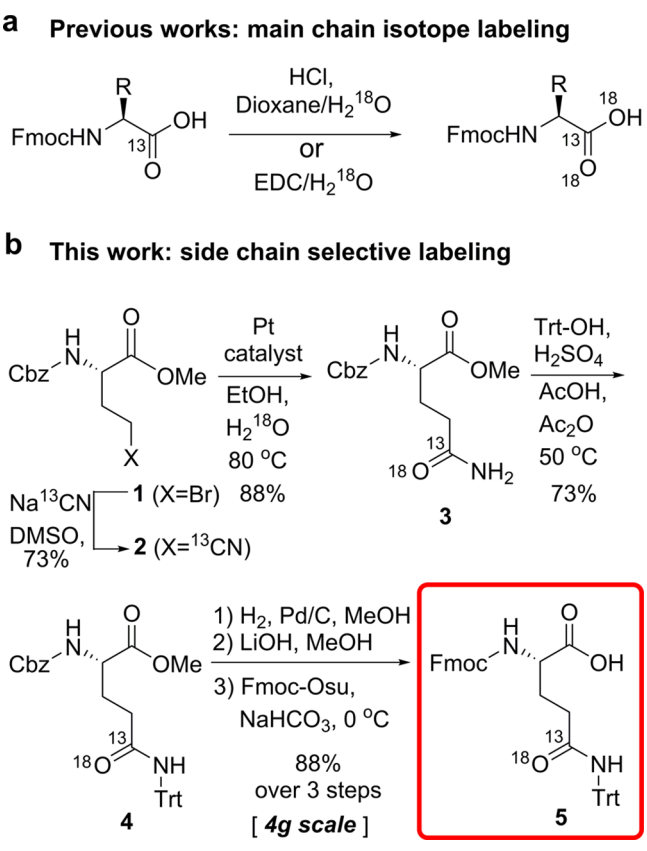

Figure 1. (a) Previously reported methods for main chain $^{13}C{=}^{18}O$ labeling. (b) New synthesis route for preparing side chain $^{13}C{=}^{18}O$-labeled glutamine.

To provide further confirmation of the successful installation of side chain $^{13}C{=}^{18}O$, we recorded the Fourier transform infrared (FTIR) spectra of labeled and unlabeled glutamine methyl ester in D_2O. As shown in Figure S2, side chain $^{13}C{=}^{18}O$ displayed a single peak at 1575 cm^{-1}, and compared to the unlabeled amide, the peak is red-shifted by 64 cm^{-1}. This shift exactly matched the previously reported value for main chain $^{13}C{=}^{18}O$.[20] Thus, for the first time, we are able to isolate the side chain amide vibrational transition from the main chain amide I band.

Probing the Gln Ladder by IR and Isotope Dilution. To test whether side chain $^{13}C{=}^{18}O$ is sensitive to its local structure and environments, we examined GNNQQNY by FTIR. This yeast prion Sup35-derived peptide forms microcrystals with a known fibril-like structure featuring a steric zipper arrangement and arrays of hydrogen-bonded glutamine side chains, known as Gln ladders (Figure 2b).[5,7] In the crystal structure, Q4 is in the steric zipper interface and forms a Gln ladder. We introduced side chain $^{13}C{=}^{18}O$ onto Q4 of GNNQQNY (underlined residue is the labeling site). The attenuated total reflection (ATR-FTIR) spectrum of GNNQQNY microcrystals display a peak at 1625 cm^{-1} and no absorption around 1685 cm^{-1} (Figure 2c), consistent with a parallel β-sheet.[5] The sharp $^{13}C{=}^{18}O$ peak at 1552 cm^{-1} differs from the broad 1575 cm^{-1} absorption of a fully hydrated $^{13}C{=}^{18}O$ (Figure S2), indicating a homogeneous environment of Q4 in the steric zipper interface. The difference in the absorption frequency can be attributed to the vibrational coupling of aligned $^{13}C{=}^{18}O$ in the Gln ladder.[49,50]

We then performed an isotope dilution experiment in which we mixed labeled and unlabeled peptides to effectively break the vibrational coupling.[50] As expected (Figure 2c), the $^{13}C{=}^{18}O$ peaks of microcrystals from isotopically diluted samples gradually blue shifted to higher frequencies as we increased the ratios of unlabeled peptides. Additionally, we observed the broadening of the isotope label with increasing ratios of the unlabeled peptide, which recapitulates the results observed in the simulated isotope dilution experiments (Figure

DOI: 10.1021/jacs.9b00577
J. Am. Chem. Soc. 2019, 141, 7320−7326

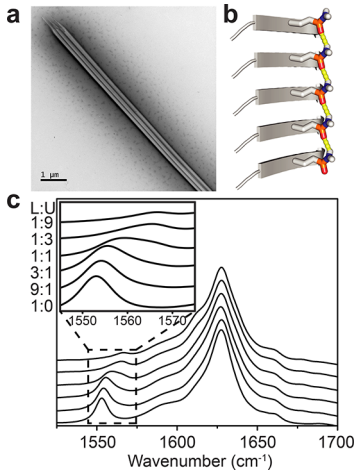

Figure 2. Isotope dilution detected Gln ladders in GNNQQNY microcrystals. (a) EM image of GNNQQNY microcrystals. Scale bar: 1 μm. (b) The alignment of side chain carbonyls to form a Gln ladder (orange). The graph was created from PDB 5K2G.[7] (c) ATR-FTIR spectra of microcrystal samples with various ratios of GNNQQNY (labeled, L) and GNNQQNY (unlabeled, U). The intensity is normalized according to the 1625 cm^{-1} peak.

S3). We calculated coupling constant β from $\nu = \nu_0 + 2\beta$, where ν and ν_0 are the frequencies of coupled and uncoupled transitions, respectively. The obtained coupling constant (−7 cm^{-1}) differs from the reported value (−9 to −11 cm^{-1}) for two hydrogen-bonded carbonyls of adjacent strands in a perfectly parallel β-sheet.[16,51,52] This deviation might reflect the difference in coupling between primary amides (side chain) and secondary amides (main chain). Another possible explanation is the contribution of positive vibrational coupling between Q4 carbonyls of mating sheets in steric zippers. In other words, two Gln ladders pack against each other. Therefore, isotope dilution is an effective and convenient way to probe Gln ladders, and analyzing the vibrational coupling constant could provide additional insights into the arrangement of ladders.

Sensitivity of the Peak Line Width to the Local Hydration Environment. We next ask whether side chain $^{13}C{=}^{18}O$ can detect the local hydration status. In GNNQQNY, although both Q4 and Q5 form Gln ladders, they experience completely different hydration environments. Q4 is in the dry steric zipper interface, while Q5 sits in the wet interface (Figure 3a). To investigate the differences, we prepared another peptide GNNQQNY with side chain $^{13}C{=}^{18}O$ on Q5. The ATR−FTIR spectrum of GNNQQNY microcrystals showed a much broader $^{13}C{=}^{18}O$ peak at 1559 cm^{-1} with the peak line width (~20 cm^{-1}) almost doubled compared to that of GNNQQNY microcrystals (~10 cm^{-1}) (Figure 3b). Because isotope dilution confirmed the ladder arrangement of Q5 (Figure S4), the peak broadening is not likely due to conformational heterogeneity. Instead, it should reflect the heterogeneous interaction of Q5 side chains with water molecules. The difference in the absorption frequency might be attributed to the differences in hydrogen bonding strength and/or the local electric field,[53,54] which would require further investigation. Nevertheless, the $^{13}C{=}^{18}O$ line width provides a convenient means to determine whether the probe is in or outside the dry steric zipper interface.

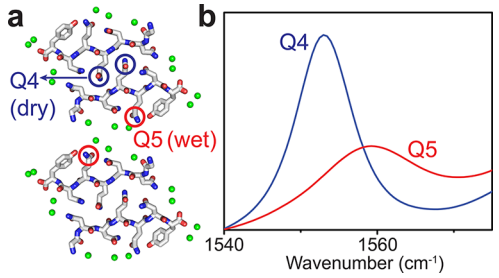

Figure 3. Peak line width is sensitive to the local hydration status. (a) In the crystal structure of GNNQQNY (PDB 5K2G), glutamine side chains are in either dry (Q4, blue) or wet interfaces (Q5, red). Green spheres represent water molecules. (b) ATR-FTIR spectra of microcrystals formed by GNNQQNY (Q4, blue) and GNNQQNY (Q5, red).

Application of $^{13}C{=}^{18}O$ to Structural and Kinetical Studies of Amyloid Fibrils. In the above studies, we demonstrated the high sensitivity of side chain $^{13}C{=}^{18}O$ using microcrystalline GNNQQNY as a model system. To begin to explore side chain $^{13}C{=}^{18}O$ in amyloid fibrils, we further studied three fibril samples formed by GNNQQNY as well as two tau-derived peptide segments, Ac-VQIVYK-NH_2 and $tau_{306-321}$. These peptides differ in their original proteins and peptide lengths. In particular, $tau_{306-321}$ is significantly longer and contains an Asp residue whose side chain carboxylate vibration could potentially overlap with Gln $^{13}C{=}^{18}O$.[56]

GNNQQNY Fibrils. In the above section, we investigated microcrystalline GNNQQNY formed at low concentrations in the presence of crystal seeds. The same peptide also forms amyloid fibrils at high concentrations, but the conformation is quite different from that in the microcrystalline form.[57,58] Using solid-state NMR (ssNMR), Griffin and co-workers have extensively studied the GNNQQNY fibril and proposed two closely related models.[55,58−60] In each of these models, the sheets pack in two distinct zipper interfaces (Figure 4b, light blue and pink). Q4 forms infinite hydrogen-bonded ladders that alternately pack with a second Q4 ladder or with another ladder from Q5. However, no other studies exist to support this packing arrangement with two distinct environments. We thus studied GNNQQNY fibrils by IR spectroscopy. As shown in Figure 4c, the amide I′ band of the fibrils displayed significantly higher complexity compared to that of microcrystals (Figure 4d). In contrast to the single $^{13}C{=}^{18}O$ peak observed in microcrystals, fibrils displayed two peaks, suggesting that Q4 side chains are in two different environments. The data are consistent with the proposed models.

Ac-VQIVYK-NH_2 Fibrils. The hexapeptide ($tau_{306-311}$) is essential to the aggregation of tau that is associated with several neurodegenerative diseases.[61,62] Eisenberg and co-workers also solved the crystal structure of this peptide, showing the class 1 steric zipper.[6] However, few studies directly support the same intersheet packing in the fibril form. We thus examined the fibril sample formed by Ac-VQIVYK-NH_2 with side chain $^{13}C{=}^{18}O$ on Q2. As shown in Figure 5b, the main amide I′ band is centered at 1618 cm^{-1}, and $^{13}C{=}^{18}O$ displays a single peak at 1575 cm^{-1}. Moreover, similar to the study with GNNQQNY microcrystals, isotope dilution caused a blue shift, which identified Gln ladders. Taken together, these results are consistent with the class 1 steric zipper in Ac-VQIVYK-NH_2 fibrils. (See also the discussion in the next section.)

DOI: 10.1021/jacs.9b00577
J. Am. Chem. Soc. 2019, 141, 7320−7326

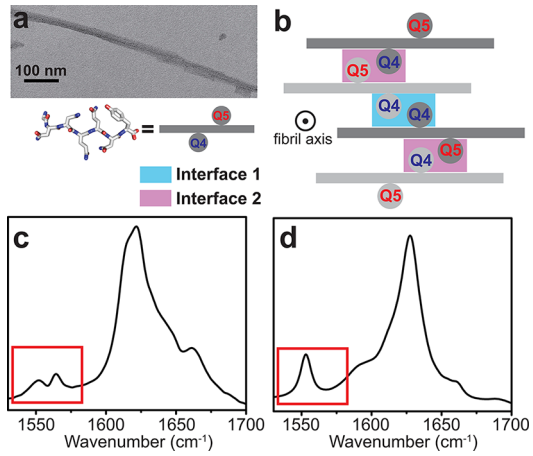

Figure 4. Characterization of GNNQQNY fibrils. (a) EM image of GNNQQNY fibrils. Scale bar: 100 nm. (b) GNNQQNY protofilament model proposed by Griffin and co-workers.[55] For clarity, side chains other than Q4 and Q5 are omitted. In the model, Q4 side chains are in two different interfaces—interface 1 (cyan) and interface 2 (pink)—which occur in a 1:1 molar ratio. A second model (not shown) proposed by Griffin and co-workers[55] has a similar structure, although the interfaces occur in different molar ratios. (c) The FTIR spectrum of fibrils is most consistent with the model shown in b and is quite distinct from what was observed in microcrystals (d) formed by the same peptide.

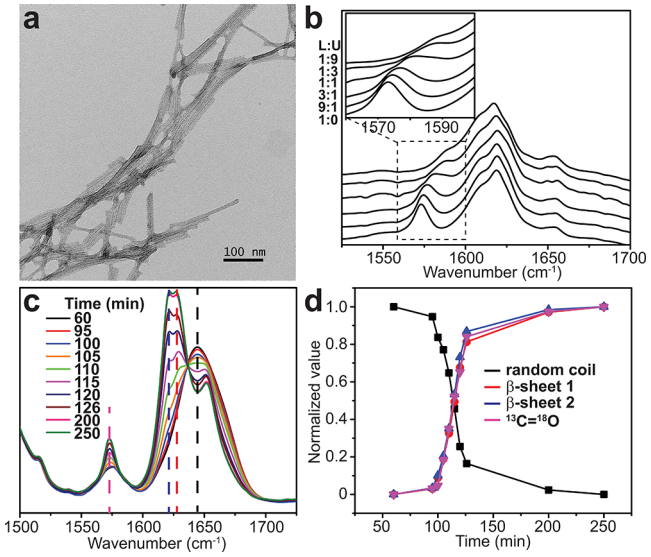

Figure 5. (a) EM image of Ac-VQIVYK-NH_2 fibrils. Scale bar: 100 nm. (b) ATR-FTIR spectra of fibril samples with various ratios of Ac-VQIVYK-NH_2 (labeled, L) and Ac-VQIVYK-NH_2 (unlabeled, U). The intensity is normalized according to the 1619 cm^{-1} peak. (c) FTIR spectra were taken following the aggregation of $tau_{306-321}$ in 1× PBS (D_2O). Dashed lines denote different structural components. Black, random coil; red, β-sheet 1; blue, β-sheet 2; magenta, Gln side chain $^{13}C{=}^{18}O$. (d) Evolution of different structural components over time. The same color code as for the dashed line is used.

Kinetics of Gln Ladder Formation in $tau_{306-321}$. We next evaluate the use of side chain $^{13}C{=}^{18}O$-labeled Gln in a longer peptide, which also includes a carboxylate-containing side chain, potentially interfering with the side chain $^{13}C{=}^{18}O$ absorption.[56] To examine these issues, we studied $tau_{306-321}$ (^{306}VQIVYKPVDLSKVTSK^{321}), a peptide fragment derived from the third repeat region of tau and containing an Asp residue.[31] This peptide aggregates within a few hours and thus is well-suited to the kinetics measurement. As shown in Figure 5c, this peptide initially adopted a random coil conformation with a broad amide I′ band centered at 1645 cm^{-1} and another broad peak at 1575 cm^{-1}, contributed by the Asp side chain and unstructured $^{13}C{=}^{18}O$. As the aggregation proceeded, the random coil component started to decrease, and the spectral signature of the β-sheet emerged. Concurrently, the 1575 cm^{-1} peak sharpened. Because no change in the 1575 cm^{-1} peak was observed in the unlabeled peptide (Figure S5), this sharpening must be associated with the alignment of side chain $^{13}C{=}^{18}O$ to form a Gln ladder. By monitoring the changes in these components over time (Figure 5d), sigmoidal curves typical of nucleation growth kinetics were observed and matched the previously reported kinetics trace by the thioflavin T (ThT) signal.[31] Interestingly, these structural changes followed similar trends, suggesting a well-concerted process involving both main chain and side chain groups during the aggregation of $tau_{306-321}$. The isosbestic point at 1636 cm^{-1} (Figure 5c) suggests a transition between two structural states (initial and final) with few intermediate species, consistent with the nucleation growth mechanism in which the nuclei grow rapidly once formed.[63] Our study represents the first investigation of Gln ladder formation during amyloid aggregation and should facilitate further investigation into this subject. Importantly, because of the homogeneity and much higher absorptivity of $^{13}C{=}^{18}O$ in Gln ladders, an Asp residue did not interfere with the analysis. We believe that, for more difficult systems containing multiple Asp/Glu residues, a side chain $^{13}C{=}^{18}O$ study is highly feasible, particularly with the aid of two-dimensional methods.

IR Information in Structural Modeling. In the absence of a high-resolution structure, IR data from side chain $^{13}C{=}^{18}O$ provides sensitive environmental information that can be used to assess alternative models of amyloid structures, thus producing a more precise final model. To demonstrate this application, we modeled amyloid protofilament structures with the open source *Integrative Modeling Platform* (IMP) program (http://integrativemodeling.org) using microcrystalline GNNQQNY as a test case (Figure 6a).

As classified by Eisenberg and co-workers, the steric zipper can be described by eight different types of packing—classes 1 to 8—depending on strand-to-strand and sheet-to-sheet arrangements.[2,3,6] Seven of the eight classes (all except class 3) have been observed experimentally. We first determined the zipper type using IR data of microcrystalline GNNQQNY (Figure 6a). As discussed above, the main amide I′ band supports parallel β-sheets, so we can rule out classes 5 to 8 that consist of antiparallel β-sheets. However, information for the main chain alone is not sufficient to further distinguish among classes 1, 2, and 4. Using side chain $^{13}C{=}^{18}O$ and isotope dilution, we identified a hydrogen-bonded array of Q4 side chains, therefore supporting in-register β-sheets. Moreover, because both Q4 and Q5 side chains showed singlet peaks, classes 2 and 4 can be eliminated; otherwise, because of the translational symmetry in classes 2 and 4, we would observe alternating solvent-exposed and solvent-buried environments for both Q4 and Q5 side chains. As a result, the class 1 steric zipper is the only one of the original eight classes that is consistent with the IR data.

Next, we generated an unbiased ensemble of GNNQQNY models that satisfy basic physical and geometrical restraints of the class 1 steric zipper using a modified version of the

DOI: 10.1021/jacs.9b00577
J. Am. Chem. Soc. 2019, 141, 7320−7326

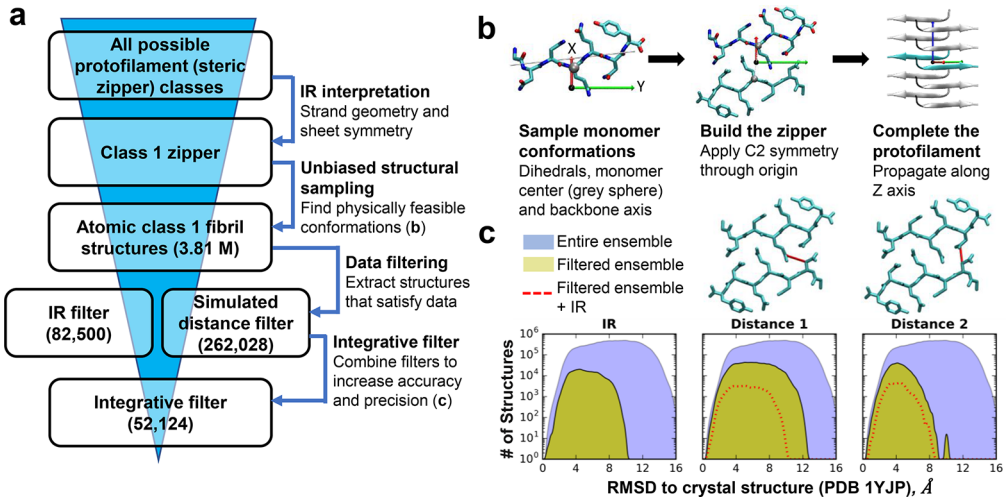

Figure 6. IR information on modeling structural ensembles of GNNQQNY. (a) Flowchart depicting how IR data was used to filter the ensemble of possible structures. (b) Building a protofilament by sampling only monomer parameters. The position of the monomer center (gray sphere) and yaw/pitch/roll of the fibril axis (gray line) are sampled along with backbone and side chain dihedral angles. The zipper was built by applying C_2 symmetry through the origin, and the protofilament was created by propagating the fibril along the Z axis. A total of 3.81 million models were generated. (c) Histograms showing the increases in accuracy and precision from data filtering using IR data and two simulated distance constraints and the integrative data filter. Fibril RMSD is defined as the sum of the all-heavy-atom RMSD of the model monomer to the crystal monomer plus the distance between the monomer centers.

kinematics module of IMP[64] to sample backbone and side chain dihedral angles and fibril geometry parameters (Figure 6b). The resulting ensemble of 3.81 million models (Figure S6, top left) was further filtered to include only those that satisfied the IR data of microcrystalline GNNQQNY, determined by the solvent-accessible surface areas of Q4 and Q5 as well as a hydrogen-bonding network along Q4 (see Table S1 for a list of the exact geometrical thresholds used). The resulting filtered ensemble (Figure S6) was significantly reduced from 3.81 million to 82 500 models (2.6% of the original ensemble). In addition, the IR filter increased the accuracy of the ensemble, defined as the fibril root-mean-square deviation (fibril RMSD, detailed in Figure 6 and the method section) of fibril models to the crystal structure (PDB 1YJP)[5], from 8.5 Å for the entire ensemble to 5.2 Å for the IR-filtered ensemble (Figure 6c, left).

Many biophysical methods, including NMR spectroscopy, can give a broad range of distance constraints. Therefore, we explore how the IR filter performs compared to distance constraints and whether they are synergistic with each other. We thus included two simulated distance constraints between two interdigitated strands of mating sheets—6 Å for N2:CB−Q4:CD (distance 1) and 5 Å for N2:CB−N6:CG (distance 2). When applied individually, these constraints provided ensemble reductions to 6.9 and 2.9% and accuracies of 6.2 and 4.3 Å, respectively (Figure 6c). The results are comparable to those from the IR filter. Importantly, combining the IR filter with distance 1 (Figure 6c, red dots) provided a further ensemble reduction to 1.4% and an increase in accuracy (1.0 Å). Integrating IR with distance 2, which is more stringent, provided a more modest gain in accuracy (0.1 Å) yet with further ensemble reduction to 0.5%. In both cases, we benefit from considering all information (integrative modeling). Interestingly, the IR information is more advantageous in determining the side chain intercalation (Figure S6) and the sheet−sheet geometry in the steric zipper, particularly because it can be used to narrow down the class of packing. These results show that the utility of information from the IR is comparable with that for a single simulated distance constraint and that the two types of constraints can be used in an integrative fashion to produce more precise and accurate structural ensembles than either type of constraint alone.

CONCLUSIONS

We report glutamine side chain $^{13}C{=}{}^{18}O$ as an intrinsic vibrational probe and its application to the study of side chain environments within amyloid fibrils. The synthesis is robust and has been achieved on a multigram scale. This non-perturbative IR probe is highly sensitive to its local environment, including the carbonyl alignment and hydration status, making it well-suited for probing the sheet-to-sheet arrangements in amyloids. We have successfully applied this probe to the studies of fibril structures and kinetics. Finally, we report a strategy of modeling amyloid structures using IR information and demonstrate the capability of integrating IR and other structural information for more accurate modeling. Thus, the combination of this sensitive IR probe and integrative modeling strategy will significantly advance IR spectroscopy in deciphering the structures and aggregation mechanisms of amyloid fibrils.

ASSOCIATED CONTENT

Supporting Information

The Supporting Information is available free of charge on the ACS Publications website at DOI: 10.1021/jacs.9b00577.

Experimental details and additional data, including Table S1 and Figures S1−S6 (PDF)

AUTHOR INFORMATION

Corresponding Authors

*hyunil.jo@ucsf.edu
*sali@salilab.org
*william.degrado@ucsf.edu

ORCID

Haifan Wu: 0000-0002-2050-9950
Huong T. Kratochvil: 0000-0001-8039-6823

DOI: 10.1021/jacs.9b00577
J. Am. Chem. Soc. 2019, 141, 7320−7326

Andrej Sali: 0000-0003-0435-6197
William F. DeGrado: 0000-0003-4745-263X

Notes

The authors declare no competing financial interest.

■ ACKNOWLEDGMENTS

This work is supported by grants from the National Institutes of Health (P01AG002132 to W.F.D. and A.S. and R35GM122603 to W.F.D.). H.W. was supported by a CTSI TL1 Postdoctoral Fellowship (TL1TR001871). H.T.K. was supported by a Ruth L. Kirschstein NRSA Postdoctoral Fellowship (F32GM125217). We thank Dr. Michael Sawaya (UCLA) for suggestions regarding the microcrystal preparation and Dr. Feng Gai (UPenn) for helpful discussions.

■ REFERENCES

(1) Chiti, F.; Dobson, C. M. Protein misfolding, functional amyloid, and human disease. *Annu. Rev. Biochem.* **2006**, *75*, 333−66.
(2) Eisenberg, D.; Jucker, M. The amyloid state of proteins in human diseases. *Cell* **2012**, *148* (6), 1188−203.
(3) Riek, R.; Eisenberg, D. S. The activities of amyloids from a structural perspective. *Nature* **2016**, *539* (7628), 227−235.
(4) Fowler, D. M.; Koulov, A. V.; Balch, W. E.; Kelly, J. W. Functional amyloid−from bacteria to humans. *Trends Biochem. Sci.* **2007**, *32* (5), 217−24.
(5) Nelson, R.; Sawaya, M. R.; Balbirnie, M.; Madsen, A. O.; Riekel, C.; Grothe, R.; Eisenberg, D. Structure of the cross-beta spine of amyloid-like fibrils. *Nature* **2005**, *435* (7043), 773−8.
(6) Sawaya, M. R.; Sambashivan, S.; Nelson, R.; Ivanova, M. I.; Sievers, S. A.; Apostol, M. I.; Thompson, M. J.; Balbirnie, M.; Wiltzius, J. J.; McFarlane, H. T.; Madsen, A. O.; Riekel, C.; Eisenberg, D. Atomic structures of amyloid cross-beta spines reveal varied steric zippers. *Nature* **2007**, *447* (7143), 453−7.
(7) Sawaya, M. R.; Rodriguez, J.; Cascio, D.; Collazo, M. J.; Shi, D.; Reyes, F. E.; Hattne, J.; Gonen, T.; Eisenberg, D. S. Ab initio structure determination from prion nanocrystals at atomic resolution by MicroED. *Proc. Natl. Acad. Sci. U. S. A.* **2016**, *113* (40), 11232−11236.
(8) Tycko, R. Solid-state NMR studies of amyloid fibril structure. *Annu. Rev. Phys. Chem.* **2011**, *62*, 279−99.
(9) Fitzpatrick, A. W. P.; Falcon, B.; He, S.; Murzin, A. G.; Murshudov, G.; Garringer, H. J.; Crowther, R. A.; Ghetti, B.; Goedert, M.; Scheres, S. H. W. Cryo-EM structures of tau filaments from Alzheimer's disease. *Nature* **2017**, *547* (7662), 185−190.
(10) Fitzpatrick, A. W.; Debelouchina, G. T.; Bayro, M. J.; Clare, D. K.; Caporini, M. A.; Bajaj, V. S.; Jaroniec, C. P.; Wang, L.; Ladizhansky, V.; Muller, S. A.; MacPhee, C. E.; Waudby, C. A.; Mott, H. R.; De Simone, A.; Knowles, T. P.; Saibil, H. R.; Vendruscolo, M.; Orlova, E. V.; Griffin, R. G.; Dobson, C. M. Atomic structure and hierarchical assembly of a cross-beta amyloid fibril. *Proc. Natl. Acad. Sci. U. S. A.* **2013**, *110* (14), 5468−73.
(11) Lu, J. X.; Qiang, W.; Yau, W. M.; Schwieters, C. D.; Meredith, S. C.; Tycko, R. Molecular structure of beta-amyloid fibrils in Alzheimer's disease brain tissue. *Cell* **2013**, *154* (6), 1257−68.
(12) Tuttle, M. D.; Comellas, G.; Nieuwkoop, A. J.; Covell, D. J.; Berthold, D. A.; Kloepper, K. D.; Courtney, J. M.; Kim, J. K.; Barclay, A. M.; Kendall, A.; Wan, W.; Stubbs, G.; Schwieters, C. D.; Lee, V. M.; George, J. M.; Rienstra, C. M. Solid-state NMR structure of a pathogenic fibril of full-length human alpha-synuclein. *Nat. Struct. Mol. Biol.* **2016**, *23* (5), 409−15.
(13) Lee, M.; Wang, T.; Makhlynets, O. V.; Wu, Y.; Polizzi, N. F.; Wu, H.; Gosavi, P. M.; Stohr, J.; Korendovych, I. V.; DeGrado, W. F.; Hong, M. Zinc-binding structure of a catalytic amyloid from solid-state NMR. *Proc. Natl. Acad. Sci. U. S. A.* **2017**, *114* (24), 6191−6196.
(14) Moran, S. D.; Zanni, M. T. How to get insight into amyloid structure and formation from infrared spectroscopy. *J. Phys. Chem. Lett.* **2014**, *5* (11), 1984−1993.
(15) Ma, J.; Pazos, I. M.; Zhang, W.; Culik, R. M.; Gai, F. Site-specific infrared probes of proteins. *Annu. Rev. Phys. Chem.* **2015**, *66*, 357−77.
(16) Kim, Y. S.; Liu, L.; Axelsen, P. H.; Hochstrasser, R. M. Two-dimensional infrared spectra of isotopically diluted amyloid fibrils from Abeta40. *Proc. Natl. Acad. Sci. U. S. A.* **2008**, *105* (22), 7720−5.
(17) Kim, Y. S.; Liu, L.; Axelsen, P. H.; Hochstrasser, R. M. 2D IR provides evidence for mobile water molecules in beta-amyloid fibrils. *Proc. Natl. Acad. Sci. U. S. A.* **2009**, *106* (42), 17751−6.
(18) Middleton, C. T.; Marek, P.; Cao, P.; Chiu, C. C.; Singh, S.; Woys, A. M.; de Pablo, J. J.; Raleigh, D. P.; Zanni, M. T. Two-dimensional infrared spectroscopy reveals the complex behaviour of an amyloid fibril inhibitor. *Nat. Chem.* **2012**, *4* (5), 355−60.
(19) Torres, J.; Adams, P. D.; Arkin, I. T. Use of a new label, (13)==(18)O, in the determination of a structural model of phospholamban in a lipid bilayer. Spatial restraints resolve the ambiguity arising from interpretations of mutagenesis data. *J. Mol. Biol.* **2000**, *300* (4), 677−85.
(20) Torres, J.; Kukol, A.; Goodman, J. M.; Arkin, I. T. Site-specific examination of secondary structure and orientation determination in membrane proteins: the peptidic (13)C = (18)O group as a novel infrared probe. *Biopolymers* **2001**, *59* (6), 396−401.
(21) Shim, S. H.; Gupta, R.; Ling, Y. L.; Strasfeld, D. B.; Raleigh, D. P.; Zanni, M. T. Two-dimensional IR spectroscopy and isotope labeling defines the pathway of amyloid formation with residue-specific resolution. *Proc. Natl. Acad. Sci. U. S. A.* **2009**, *106* (16), 6614−9.
(22) Buchanan, L. E.; Dunkelberger, E. B.; Tran, H. Q.; Cheng, P. N.; Chiu, C. C.; Cao, P.; Raleigh, D. P.; de Pablo, J. J.; Nowick, J. S.; Zanni, M. T. Mechanism of IAPP amyloid fibril formation involves an intermediate with a transient beta-sheet. *Proc. Natl. Acad. Sci. U. S. A.* **2013**, *110* (48), 19285−90.
(23) Buchanan, L. E.; Carr, J. K.; Fluitt, A. M.; Hoganson, A. J.; Moran, S. D.; de Pablo, J. J.; Skinner, J. L.; Zanni, M. T. Structural motif of polyglutamine amyloid fibrils discerned with mixed-isotope infrared spectroscopy. *Proc. Natl. Acad. Sci. U. S. A.* **2014**, *111* (16), 5796−801.
(24) Nagy-Smith, K.; Beltramo, P. J.; Moore, E.; Tycko, R.; Furst, E. M.; Schneider, J. P. Molecular, local, and network-level basis for the enhanced stiffness of hydrogel networks formed from coassembled racemic peptides: predictions from Pauling and Corey. *ACS Cent. Sci.* **2017**, *3* (6), 586−597.
(25) Oh, K. I.; Lee, J. H.; Joo, C.; Han, H.; Cho, M. Beta-azidoalanine as an IR probe: application to amyloid Abeta(16−22) aggregation. *J. Phys. Chem. B* **2008**, *112* (33), 10352−7.
(26) Pazos, I. M.; Ghosh, A.; Tucker, M. J.; Gai, F. Ester carbonyl vibration as a sensitive probe of protein local electric field. *Angew. Chem., Int. Ed.* **2014**, *53* (24), 6080−4.
(27) Gao, Y. C.; Zou, Y.; Ma, Y.; Wang, D.; Sun, Y.; Ma, G. Infrared probe technique reveals a millipede-like structure for Abeta(8−28) Amyloid Fibril. *Langmuir* **2016**, *32* (4), 937−946.
(28) Jia, B.; Sun, Y.; Yang, L.; Yu, Y.; Fan, H.; Ma, G. A structural model of the hierarchical assembly of an amyloid nanosheet by an infrared probe technique. *Phys. Chem. Chem. Phys.* **2018**, *20* (43), 27261−27271.
(29) Pazos, I. M.; Ma, J.; Mukherjee, D.; Gai, F. Ultrafast hydrogen-bonding dynamics in amyloid fibrils. *J. Phys. Chem. B* **2018**, *122* (49), 11023−11029.
(30) Adhikary, R.; Zimmermann, J.; Dawson, P. E.; Romesberg, F. E. IR probes of protein microenvironments: utility and potential for perturbation. *ChemPhysChem* **2014**, *15* (5), 849−53.
(31) Stohr, J.; Wu, H.; Nick, M.; Wu, Y.; Bhate, M.; Condello, C.; Johnson, N.; Rodgers, J.; Lemmin, T.; Acharya, S.; Becker, J.; Robinson, K.; Kelly, M. J. S.; Gai, F.; Stubbs, G.; Prusiner, S. B.; DeGrado, W. F. A 31-residue peptide induces aggregation of tau's microtubule-binding region in cells. *Nat. Chem.* **2017**, *9* (9), 874−881.
(32) Martial, B.; Lefevre, T.; Auger, M. Understanding amyloid fibril formation using protein fragments: structural investigations via

DOI: 10.1021/jacs.9b00577
J. Am. Chem. Soc. 2019, 141, 7320−7326

vibrational spectroscopy and solid-state NMR. *Biophys. Rev.* **2018**, *10* (4), 1133−1149.
(33) Gallagher-Jones, M.; Glynn, C.; Boyer, D. R.; Martynowycz, M. W.; Hernandez, E.; Miao, J.; Zee, C. T.; Novikova, I. V.; Goldschmidt, L.; McFarlane, H. T.; Helguera, G. F.; Evans, J. E.; Sawaya, M. R.; Cascio, D.; Eisenberg, D. S.; Gonen, T.; Rodriguez, J. A. Sub-angstrom cryo-EM structure of a prion protofibril reveals a polar clasp. *Nat. Struct. Mol. Biol.* **2018**, *25* (2), 131−134.
(34) Davies, S. W.; Turmaine, M.; Cozens, B. A.; DiFiglia, M.; Sharp, A. H.; Ross, C. A.; Scherzinger, E.; Wanker, E. E.; Mangiarini, L.; Bates, G. P. Formation of neuronal intranuclear inclusions underlies the neurological dysfunction in mice transgenic for the HD mutation. *Cell* **1997**, *90* (3), 537−48.
(35) Michelitsch, M. D.; Weissman, J. S. A census of glutamine/asparagine-rich regions: implications for their conserved function and the prediction of novel prions. *Proc. Natl. Acad. Sci. U. S. A.* **2000**, *97* (22), 11910−5.
(36) Perutz, M. F.; Pope, B. J.; Owen, D.; Wanker, E. E.; Scherzinger, E. Aggregation of proteins with expanded glutamine and alanine repeats of the glutamine-rich and asparagine-rich domains of Sup35 and of the amyloid beta-peptide of amyloid plaques. *Proc. Natl. Acad. Sci. U. S. A.* **2002**, *99* (8), 5596−600.
(37) Kurt, T. D.; Aguilar-Calvo, P.; Jiang, L.; Rodriguez, J. A.; Alderson, N.; Eisenberg, D. S.; Sigurdson, C. J. Asparagine and glutamine ladders promote cross-species prion conversion. *J. Biol. Chem.* **2017**, *292* (46), 19076−19086.
(38) Wattendorff, A. R.; Bots, G. T.; Went, L. N.; Endtz, L. J. Familial cerebral amyloid angiopathy presenting as recurrent cerebral haemorrhage. *J. Neurol. Sci.* **1982**, *55* (2), 121−35.
(39) Abrahamson, M.; Jonsdottir, S.; Olafsson, I.; Jensson, O.; Grubb, A. Hereditary cystatin C amyloid angiopathy: identification of the disease-causing mutation and specific diagnosis by polymerase chain reaction based analysis. *Hum. Genet.* **1992**, *89* (4), 377−380.
(40) Adegbuyiro, A.; Sedighi, F.; Pilkington, A. W. t.; Groover, S.; Legleiter, J. Proteins containing expanded polyglutamine tracts and neurodegenerative disease. *Biochemistry* **2017**, *56* (9), 1199−1217.
(41) Webb, B.; Viswanath, S.; Bonomi, M.; Pellarin, R.; Greenberg, C. H.; Saltzberg, D.; Sali, A. Integrative structure modeling with the Integrative Modeling Platform. *Protein Sci.* **2018**, *27* (1), 245−258.
(42) Marecek, J.; Song, B.; Brewer, S.; Belyea, J.; Dyer, R. B.; Raleigh, D. P. A simple and economical method for the production of 13C,18O-labeled Fmoc-amino acids with high levels of enrichment: applications to isotope-edited IR studies of proteins. *Org. Lett.* **2007**, *9* (24), 4935−7.
(43) Seyfried, M. S.; Lauber, B. S.; Luedtke, N. W. Multiple-turnover isotopic labeling of Fmoc- and Boc-protected amino acids with oxygen isotopes. *Org. Lett.* **2010**, *12* (1), 104−6.
(44) Abaskharon, R. M.; Brown, S. P.; Zhang, W.; Chen, J.; Smith, A. B., 3rd; Gai, F. Isotope-labeled aspartate sidechain as a non-perturbing infrared probe: Application to Investigate the Dynamics of a Carboxylate Buried Inside a Protein. *Chem. Phys. Lett.* **2017**, *683*, 193−198.
(45) Ghaffar, T.; Parkins, A. W. A new homogeneous platinum-containing catalyst for the hydrolysis of nitriles. *Tetrahedron Lett.* **1995**, *36* (47), 8657−8660.
(46) Richter, M. J. R.; Schneider, M.; Brandstatter, M.; Krautwald, S.; Carreira, E. M. Total synthesis of (-)-Mitrephorone A. *J. Am. Chem. Soc.* **2018**, *140* (48), 16704−16710.
(47) Mercado-Marin, E. V.; Garcia-Reynaga, P.; Romminger, S.; Pimenta, E. F.; Romney, D. K.; Lodewyk, M. W.; Williams, D. E.; Andersen, R. J.; Miller, S. J.; Tantillo, D. J.; Berlinck, R. G. S.; Sarpong, R. Total synthesis and isolation of citrinalin and cyclopiamine congeners. *Nature* **2014**, *509* (7500), 318−324.
(48) Hirooka, Y.; Ikeuchi, K.; Kawamoto, Y.; Akao, Y.; Furuta, T.; Asakawa, T.; Inai, M.; Wakimoto, T.; Fukuyama, T.; Kan, T. Enantioselective synthesis of SB-203207. *Org. Lett.* **2014**, *16* (6), 1646−9.
(49) Silva, R. A.; Barber-Armstrong, W.; Decatur, S. M. The organization and assembly of a beta-sheet formed by a prion peptide in solution: an isotope-edited FTIR study. *J. Am. Chem. Soc.* **2003**, *125* (45), 13674−5.
(50) Paul, C.; Wang, J.; Wimley, W. C.; Hochstrasser, R. M.; Axelsen, P. H. Vibrational coupling, isotopic editing, and beta-sheet structure in a membrane-bound polypeptide. *J. Am. Chem. Soc.* **2004**, *126* (18), 5843−50.
(51) Choi, J. H.; Ham, S. Y.; Cho, M. Local amide I mode frequencies and coupling constants in polypeptides. *J. Phys. Chem. B* **2003**, *107* (34), 9132−9138.
(52) Dunkelberger, E. B.; Buchanan, L. E.; Marek, P.; Cao, P.; Raleigh, D. P.; Zanni, M. T. Deamidation accelerates amyloid formation and alters amylin fiber structure. *J. Am. Chem. Soc.* **2012**, *134* (30), 12658−67.
(53) Bakker, H. J.; Skinner, J. L. Vibrational spectroscopy as a probe of structure and dynamics in liquid water. *Chem. Rev.* **2010**, *110* (3), 1498−517.
(54) Wang, L.; Middleton, C. T.; Zanni, M. T.; Skinner, J. L. Development and validation of transferable amide I vibrational frequency maps for peptides. *J. Phys. Chem. B* **2011**, *115* (13), 3713−24.
(55) Lewandowski, J. R.; van der Wel, P. C.; Rigney, M.; Grigorieff, N.; Griffin, R. G. Structural complexity of a composite amyloid fibril. *J. Am. Chem. Soc.* **2011**, *133* (37), 14686−98.
(56) Barth, A. The infrared absorption of amino acid side chains. *Prog. Biophys. Mol. Biol.* **2000**, *74* (3−5), 141−73.
(57) Balbirnie, M.; Grothe, R.; Eisenberg, D. S. An amyloid-forming peptide from the yeast prion Sup35 reveals a dehydrated beta-sheet structure for amyloid. *Proc. Natl. Acad. Sci. U. S. A.* **2001**, *98* (5), 2375−80.
(58) van der Wel, P. C.; Lewandowski, J. R.; Griffin, R. G. Solid-state NMR study of amyloid nanocrystals and fibrils formed by the peptide GNNQQNY from yeast prion protein Sup35p. *J. Am. Chem. Soc.* **2007**, *129* (16), 5117−30.
(59) Debelouchina, G. T.; Bayro, M. J.; van der Wel, P. C.; Caporini, M. A.; Barnes, A. B.; Rosay, M.; Maas, W. E.; Griffin, R. G. Dynamic nuclear polarization-enhanced solid-state NMR spectroscopy of GNNQQNY nanocrystals and amyloid fibrils. *Phys. Chem. Chem. Phys.* **2010**, *12* (22), 5911−9.
(60) van der Wel, P. C.; Lewandowski, J. R.; Griffin, R. G. Structural characterization of GNNQQNY amyloid fibrils by magic angle spinning NMR. *Biochemistry* **2010**, *49* (44), 9457−69.
(61) von Bergen, M.; Friedhoff, P.; Biernat, J.; Heberle, J.; Mandelkow, E. M.; Mandelkow, E. Assembly of tau protein into Alzheimer paired helical filaments depends on a local sequence motif ((306)VQIVYK(311)) forming beta structure. *Proc. Natl. Acad. Sci. U. S. A.* **2000**, *97* (10), 5129−34.
(62) Mandelkow, E. M.; Mandelkow, E. Biochemistry and cell biology of tau protein in neurofibrillary degeneration. *Cold Spring Harbor Perspect. Med.* **2012**, *2* (7), a006247.
(63) Jarrett, J. T.; Lansbury, P. T., Jr. Seeding "one-dimensional crystallization" of amyloid: a pathogenic mechanism in Alzheimer's disease and scrapie? *Cell* **1993**, *73* (6), 1055−8.
(64) Carter, L.; Kim, S. J.; Schneidman-Duhovny, D.; Stohr, J.; Poncet-Montange, G.; Weiss, T. M.; Tsuruta, H.; Prusiner, S. B.; Sali, A. Prion protein-antibody complexes characterized by chromatography-coupled small-angle x-ray scattering. *Biophys. J.* **2015**, *109* (4), 793−805.

DOI: 10.1021/jacs.9b00577
J. Am. Chem. Soc. 2019, 141, 7320−7326